Journal of Physics:
Conference Series

PAPER • **OPEN ACCESS**

Experimental Analysis of Noise Intermittency Induced by Tandem Rotor Aeroacoustic Interference

To cite this article: T. Pagliaroli *et al* 2025 *J. Phys.: Conf. Ser.* **3063** 012005

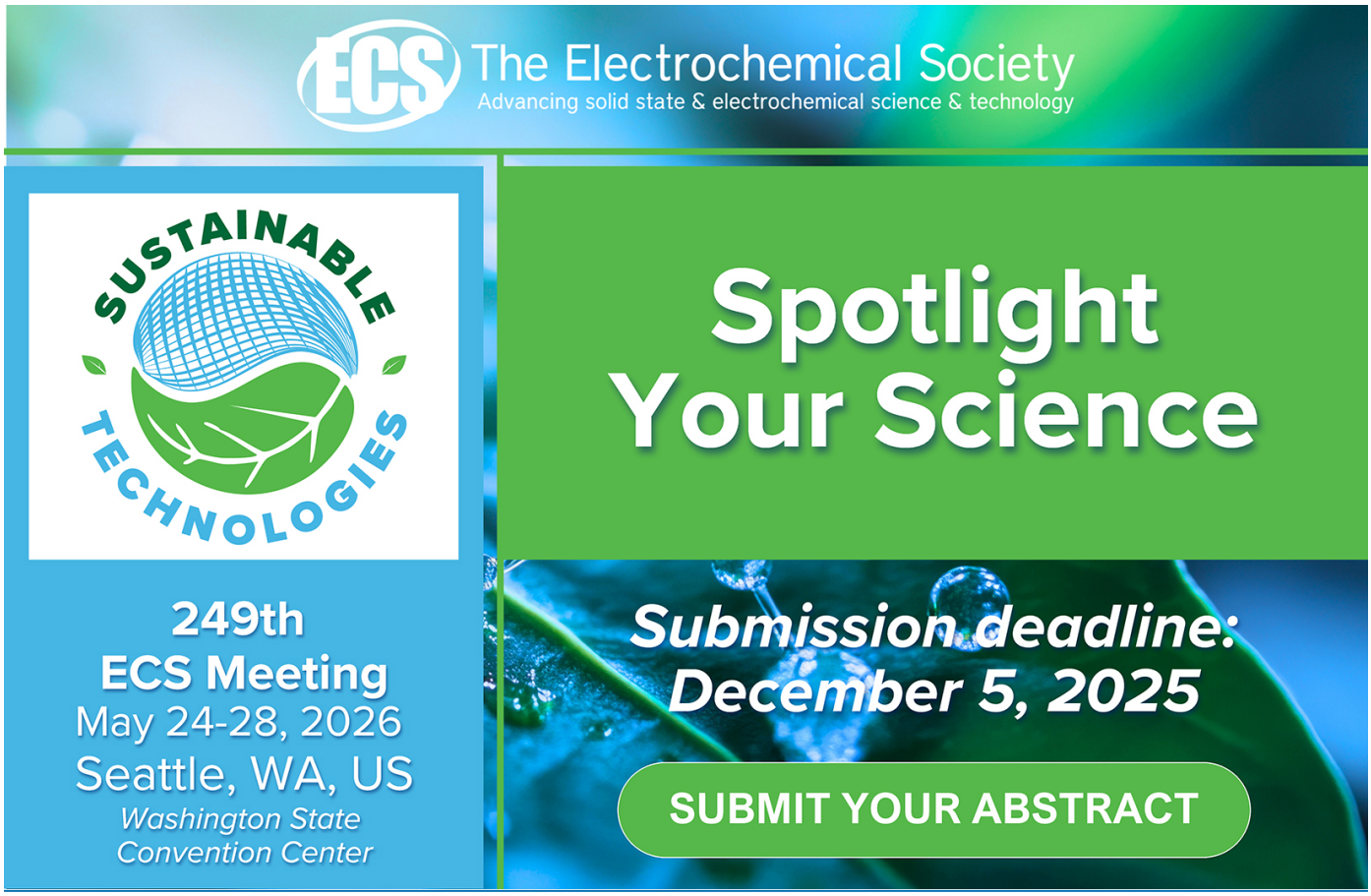

Journal of Physics: Conference Series **3063** (2025) 012005 doi:10.1088/1742-6596/3063/1/012005

Experimental Analysis of Noise Intermittency Induced by Tandem Rotor Aeroacoustic Interference

T. Pagliaroli[1], P. Candeloro[1], F. Del Duchetto[1], J. Yin[2] and K.-S. Rossignol[2]

[1]Department of Engineering, University Niccolò Cusano, Rome, Italy
[2]DLR German Aerospace Center, Braunschweig, Germany

E-mail: tiziano.pagliaroli@unicusano.it

Abstract.

This study investigates the aeroacoustic effects of phase synchronization between co-rotating propellers in side-by-side configurations. Time-domain Proper Orthogonal Decomposition (POD) is employed on pressure fluctuation data to separate tonal and broadband components, enabling a detailed analysis of acoustic interference mechanisms.
Experimental results demonstrate that synchronization significantly influences the tonal component, highlighting distinct regimes of constructive and destructive interference depending on the rotor phase delay. Specifically, the analysis reveals a notable reduction in noise amplitude at specific phase shifts, particularly affecting the second harmonic. An explanation of this scientific outcome is provided and illustrated schematically.
Additionally, probability density functions indicate pronounced modifications in the statistical characteristics of pressure fluctuations related to phase synchronization, further supporting the effectiveness of the decomposition approach. he results demonstrate the effectiveness of rotor synchronization as a useful active noise control strategy in order to achieve a significant noise mitigation.
A non-linear analysis is applied to the tonal component, revealing a path to chaos via intermittency during the transition between constructive and destructive interference. More in detail, a local birth and death of periodic oscillations via Hopf-like bifurcation is observed. This aspect highlights the intricate and fascinating chaotic nature of the interference transition. The chaotic behavior of the tonal component is related to the macro time scale of the pressure fluctuation, and has been incorporated into the mathematical model.

1 Introduction

U-space fosters drones integration into European airspace; however, noise pollution remains a significant barrier to public acceptance [10]. While research on isolated rotor noise has advanced [4], multirotor configurations necessitate a more comprehensive aeroacoustic framework [10, 15, 21]. Passive noise control strategies, such as serrated propeller edges [5, 6, 22], often compromise aerodynamic efficiency [32], whereas active noise cancellation systems introduce additional weight and complexity [9]. In this context, rotor phase synchronization has emerged as a promising alternative, mitigating acoustic emissions without aerodynamic penalties [9]. The key-idea is to manipulate phase angles between rotors to induce destructive acoustic interference [7], leading to three primary effects: reduction in noise amplitude, modulation of acoustic signatures, and alteration of directivity patterns. Rotor synchronization can achieve

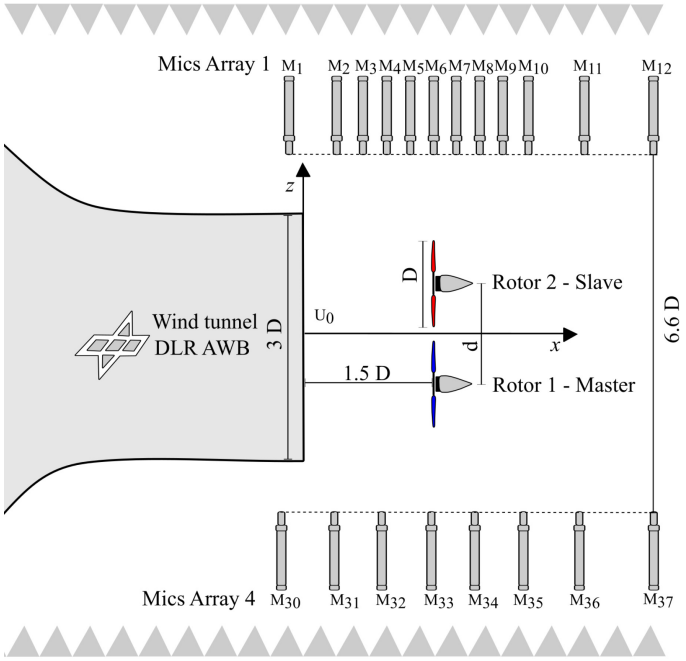

Figure 1: Microphone layout.

significant noise reductions at blade passage frequency [12, 14, 27, 32, 33, 35], with co-rotating rotors benefiting more substantially than counter-rotating configurations [30]. Directivity modifications depend on phase differences, resulting in shifts between monopole and dipole radiation patterns [8, 25, 26]. Additionally, modulation effects introduce intermittent wave packets into pressure time histories [8, 35]. The present study employs time domain Proper Orthogonal Decomposition (POD) to separate the pressure fluctuations field, sampled by linear microphone array, into tonal and broadband components. This decomposition facilitates an in-depth analysis of the tonal component, typically the most annoying, offering detailed insights into the acoustic interference mechanisms between co-rotating rotors arranged in a side-by-side configuration.

The paper is structured as follows. Section §2 describes the experimental setup, instrumentation, and operating conditions. The rotor acoustic interference phenomena are analyzed and discussed in Section §3. Finally, the main conclusions are summarized in Section §4.

2 Experimental Setup

The tests were performed in the Acoustic Wind Tunnel Braunschweig (AWB) optimised for noise measurements above 250 Hz. In the present analysis, the wind tunnel was deactivated during the tests to simulate hovering conditions. A total of 37 microphones were deployed in four non-equidistant linear arrays, with only arrays 1 and 4 used in this study. The acoustic signals were acquired at 102 kHz for 30 s per operating point. The microphones layout is depicted in Figure 1.

The setup comprised three-bladed KDE-CF155-TP propellers ($15.5'' \times 5.3$) mounted on vertical supports with adjustable spacing (d). The propellers is characterized by a diameter $D = 393.7\,\text{mm}$ and a mean aerodynamic chord $c = 28.5\,\text{mm}$. KDE4012XF-400 motors, controlled by KDEXF-UAS55 electronic speed controllers, powered the propellers. The two microphone arrays were positioned at $3.3D$ from the x-axis, ensuring pressure amplitudes were purely acoustic ($p' \propto 1/r$).

A custom synchrophaser was developed to control the phase delay, $\psi(t)$, between co-rotating rotors operating at a rotational speed $\omega(t)$. The rotors were configured in a master–slave arrangement, where a PID controller regulated the phase shift by adjusting the slave rotor relative to the master every 5 ms. The synchrophaser ensured stable rotational speeds and precise phase shift throughout the operation. The system employed an incremental encoder Kübler 05.2400 with 500 pulses per revolution and National Instruments NI PXI-1031 chassis equipped with a NI PXI-7350 motion controller, and a NI PXI-6259 multifunction DAQ.

Experiments were conducted in hover conditions with phase differences varied in 15° increments. The

mutual rotor distance tested was $d/D = 1.20$, to maximize interactional effects, with the rotational speed fixed at 5200 RPM. Several test cases were analysed, including an isolated rotor reference case. The blade tip Mach number was $M_{\text{tip}} = 0.31$, and the Reynolds number at 75% span was $Re_{c75} = 1.51 \times 10^5$.

3 Results

3.1 Tonal and broand-band noise separation

The propellers noise is tipically splitted into two main components: tonal (narrow-band) and broadband noise. Tonal noise originates from the periodic blade motion, related directly to blade rotation speed, thickness, and aerodynamic loading. Conversely, the broadband counterpart arises from turbulent structures and their interaction with blade edges, exhibiting random, incoherent characteristics in both space and time. The separation of these noise components is crucial for experimental analysis and validating simulations based on the Ffowcs Williams–Hawkings equation. Recent studies have introduced various separation techniques [2, 3, 20, 31].

The only-time POD technique proposed by Candeloro et al. [6] utilizes a single microphone and enables the separation of coherent and stochastic components through a truncated Proper Orthogonal Decomposition (POD) expansion. This method offers several key advantages, including straightforward implementation, low sensitivity to the selection of the truncation threshold, and robustness with respect to the time window size. By applying the only-time POD decomposition technique to the raw pressure data were splitted into tonal and broadband components. In Figure 2 the tonal component, in the b and e figures, was notably smoother and perfectly in phase with the raw signal, reported in the a and d figures. Conversely, the broadband component, illustrated in Figure 2(c), displays the characteristic behavior typically associated with white noise.

Moreover, Figure 3 presents the calculated Sound Pressure Spectral Level (SPSL), demonstrating that the coherent component spectrum aligns with the first three harmonics of the raw signal and remains nearly flat across the normalized frequency range $f/f^* \in [0.1, 1)$. Additionally, this decomposition technique effectively removes intermediate peaks between harmonics observed in the raw signal, distinguishing it from conventional band-pass filters. Tthe probability density function (PDF) of the incoherent signal is reported in Figure 4 and it closely follows a Gaussian distribution up to 3σ, confirming its stochastic nature. Conversely, the PDF of the coherent component is characterised by a bi-modal distribution, with peaks corresponding to blade passage events. These distinct PDF shapes validate the effectiveness of the decomposition technique in properly decoupling tonal and broadband noise components.

3.2 Acoustic pre-qualification of the time series

Figure 5 illustrates the effect of varying phase delay (ψ) between side-by-side rotors. At $\psi = 0°$ (Figure 5a), pairs of red-blue streaks appear for each blade passing period, with the delay between waves determined solely by rotor spacing. Increasing the phase delay to $\psi = 45°$ results in the alignment of compression waves from both rotors, producing constructive interference (Figure 5d). Conversely, at intermediate angles such as $\psi = 15°$ and $75°$, destructive interference occurs due to the overlap between expansion and compression waves, significantly reducing fluctuation amplitude. In Figure 6 is depicted pressure fluctuation time series showing the interference mechanism between side-by-side rotors for different phase delays (ψ). The same cases has been of Figure 5 has been considered to further highlight the different behaviours. Figure 7 depict the Overall Sound Pressure Level (OASPL) for varying phase delays (ψ) between side-by-side rotors, comparing these results to the noise radiated by an isolated propeller, represented by the dotted line. This figure reveals promising findings, particularly at angles associated with destructive interference ($\psi = 15°$ and $\psi = 75°$), where the noise produced by two synchronized rotors is notably lower than that of a single rotor. Conversely, constructive interference, observed at $\psi = 45°$, significantly increases the noise level. These findings confirm the potential of rotor synchronisation in effectively reducing aerodynamic noise through controlled interference. A further investigation in the Fourier domain is conducted, focusing on the cases with $\psi = 0°$, $\psi = 45°$ and $\psi = 75°$. In Figure 8, the first harmonic is notably higher under constructive interference than in other cases. Consistent with [11, 23], the second harmonic experiences the most significant mitigation due to destructive interference as reported in Table 1. Figure 6(f) clarifies why the second harmonic is mitigated: synchronisation of compression and expansion waves cancels fluctuations, resulting in a compression-expansion wave with reduced periodicity, as depicted by the grey-coloured fluctuation. Furthermore, the PDFs of pressure fluctuations provides valuable insights into how pressure signals change with varying phase delays. In Figure 9, at $\psi = 0°$, the PDF exhibits a distinct bi-modal distribution, clearly identifying two constant-intensity pressure fluctuations (expansion and compression). At $\psi = 45°$, these peaks shift outward, accompanied by the emergence of two lower-intensity internal peaks, ascribed to installation

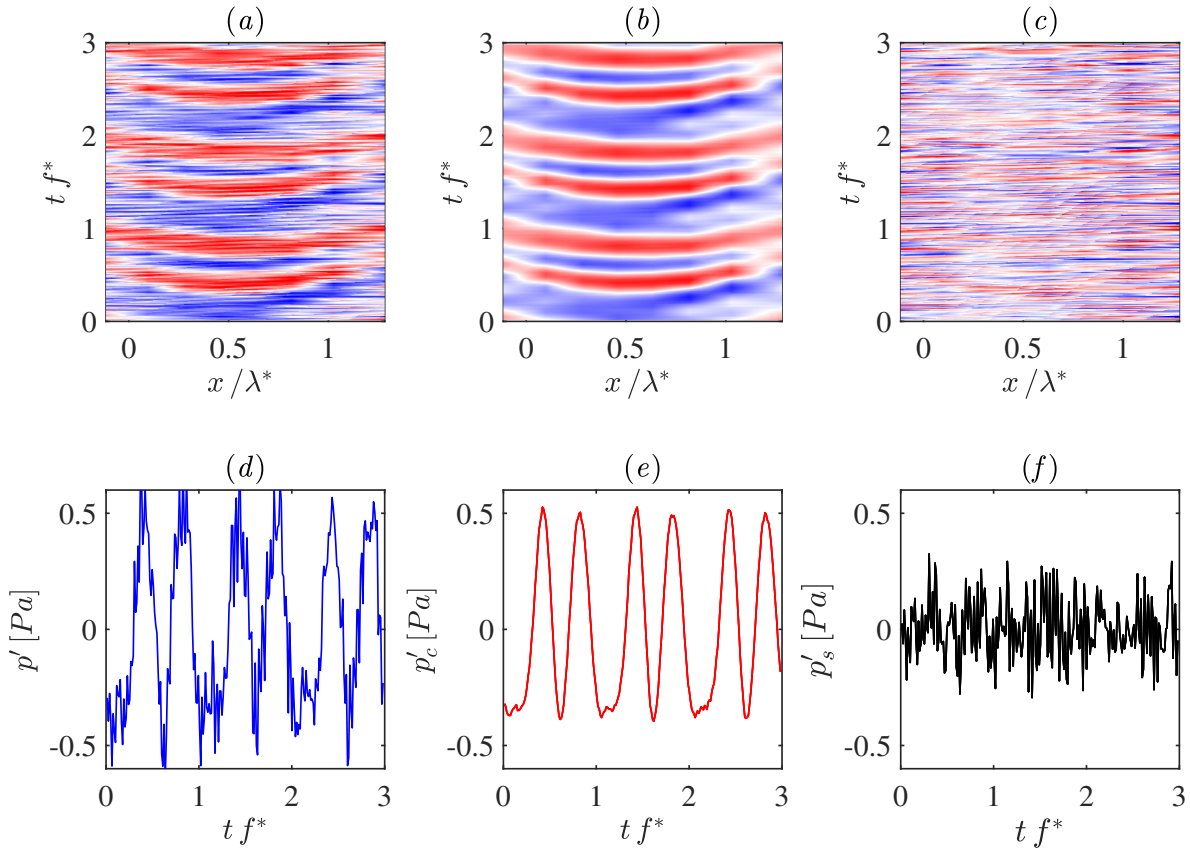

Figure 2: Input-output of theonly-time POD decomposition applied to side-by-side rotor for constant phase delay $\psi = 0°$. The first column shows the raw data (a, d), the second column presents the tonal component (b, e), and the third column the broadband component (c, f). The top row depicts the space–time fields, whereas the bottom row illustrates a representative time series at x/λ=0.45, corresponding to a location within the rotor plane.

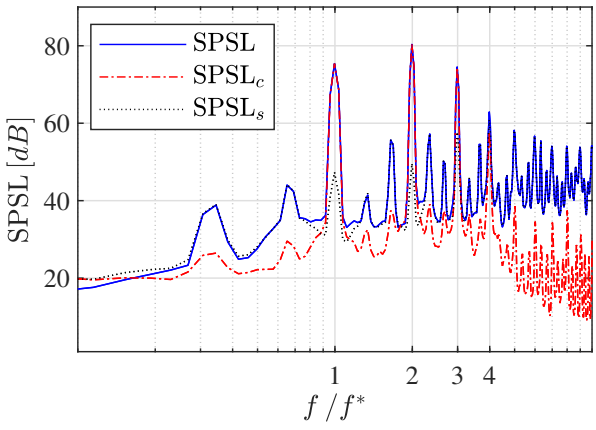

Figure 3: Sound pressure spectral levels calculated at $x/\lambda^* = 0.45$ for the raw data, tonal and broadband components.

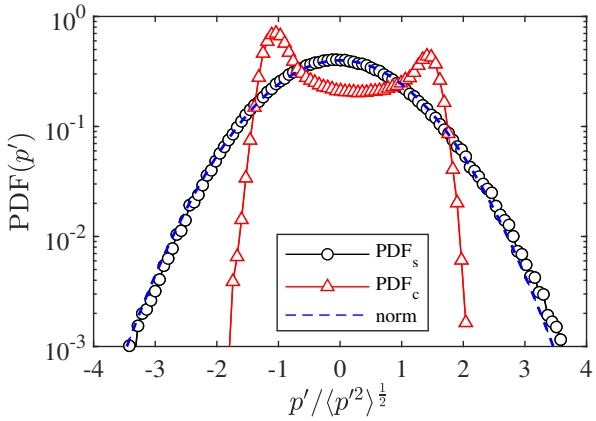

Figure 4: Probability density function of tonal and stochastic components of the pressure fluctuation.

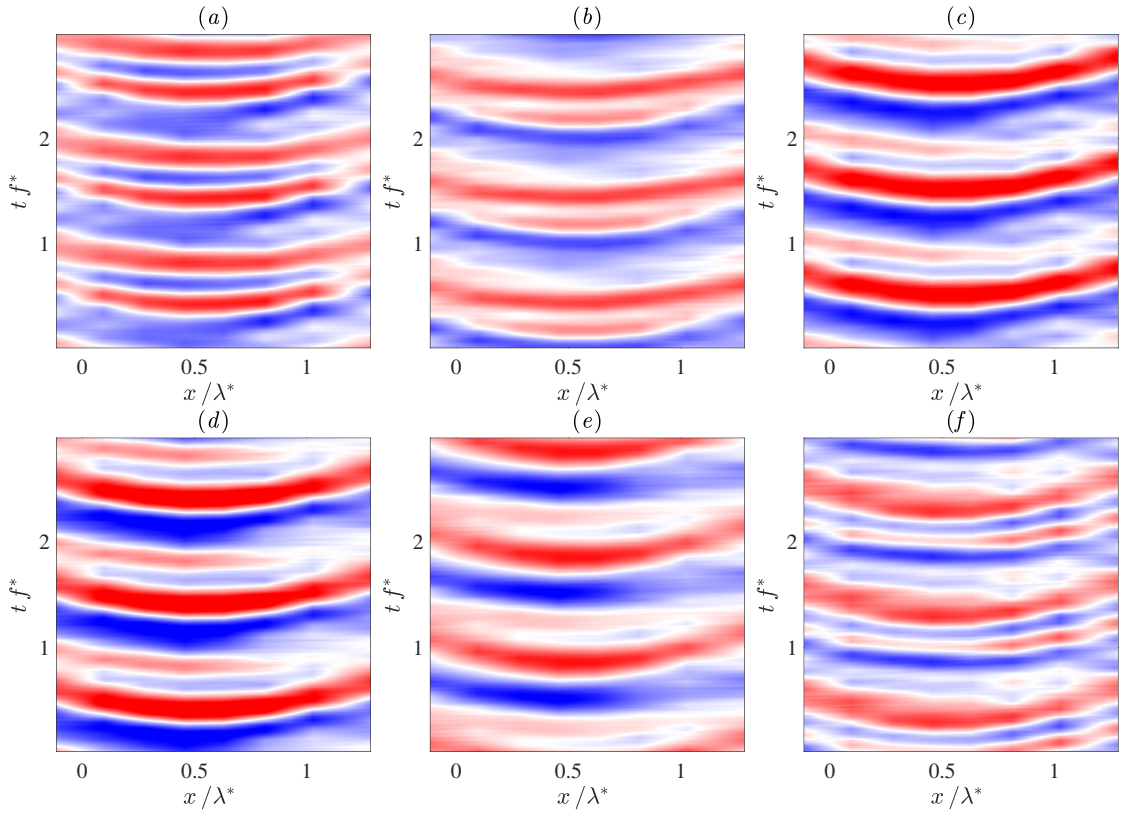

Figure 5: Pressure fluctuation space-time fields for side-by-side rotors with varying phase delays (ψ): (a) $\psi = 0°$, (b) $\psi = 15°$, (c) $\psi = 30°$, (d) $\psi = 45°$, (e) $\psi = 60°$, and (f) $\psi = 75°$.

Table 1: Sound Pressure spectral Level of the first and second harmonics by varying the rotor phase delay.

ψ, deg	$SPSL_1\,[dB]$	$SPSL_2\,[dB]$
0	75,3	74,4
45	82,2	82,4
75	79,6	62,4

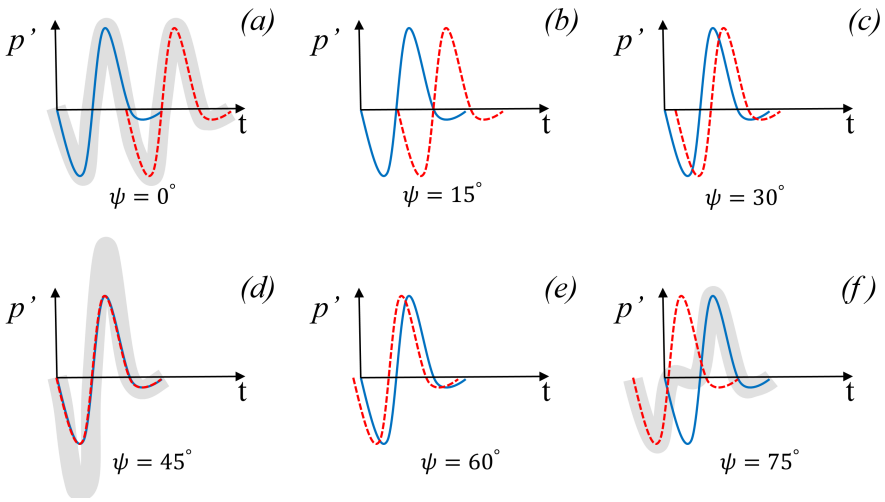

Figure 6: Schematic depiction of pressure fluctuation time series showing the interference effect between side-by-side rotors for different phase delays (ψ).

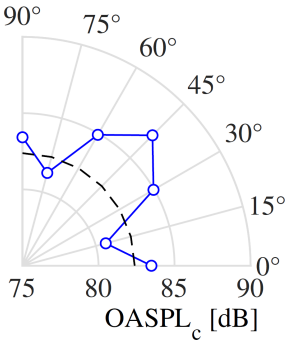

Figure 7: Overall Sound Pressure Level (OASPL) as a function of the phase delay (ψ). The dashed quarter circle represents the OASPL radiated by an isolated rotor, providing a comparative reference for evaluating the effects of rotor interactions.

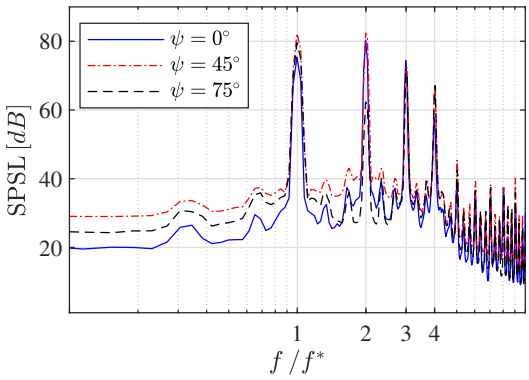

Figure 8: Sound pressure Spectra Level of the tonal component calculated for $\psi = 0°, 45°, \text{and} 75°$.

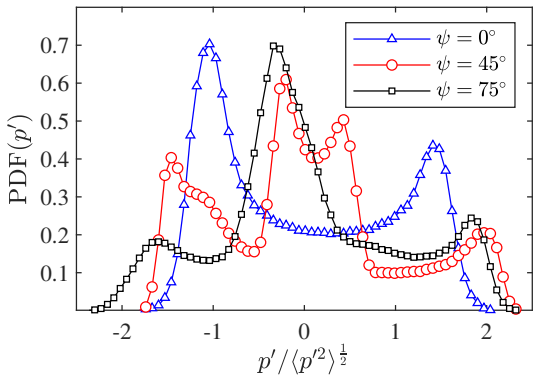

Figure 9: Probability Density Functions (PDFs) calculated ofr three condition: $\psi = 0°, 45°,$ and$75°$.

effects. At $\psi = 75°$, the PDF is dominated by a single expansion peak with an intensity very close to zero. This characteristic represents the acoustic footprint of noise cancellation due to destructive interference. Indeed, as illustrated in Figure 6f, the primary effect of destructive interference is the replacement of the positive-negative oscillation (see red and blue curves) with an extended sequence of values close to zero.

3.3 Noise intermittency: a short introduction

The phenomenon of intermittency and the chaotic nature of pressure fluctuations has been extensively investigated in the context of thermoacoustic instability [13, 16, 17], primarily through time–frequency analysis and recurrence quantification methods. However, to date, there is a lack of comprehensive studies specifically addressing rotor noise intermittency.

Intermittency is one of the typical routes to chaos, manifesting as a dynamical system's irregular alternation between bursts of chaotic activity and intervals of steady or periodic behavior [18, 24].

In fluid dynamics, the term *intermittency* was introduced to describe signals that fluctuate between flat and bursting behaviour commonly interpreted as laminar and turbulent regimes, respectively [28].Several criteria for classifying intermittency have been proposed in the literature. A widely adopted classification system was introduced by [1,29], who categorize three classes of intermittency with a different bifurcation scenario: *i)* Type I, intermittency related to a saddle-node bifurcation; *ii)* Type II, intermittency due to a Hopf bifurcation, identified by the appearance of a quasi-periodic state; *iii)* Type III, intermittency related to a reverse–period doubling bifurcation.

The following analysis was conducted focusing the attention on four specific operating conditions using microphone number 33 ($z < 0$), for the microphone position see Figure 1 :

1. isolated rotor as a reference;
2. $\psi_m = 15°$ and $d/D = 1.20$ related to the destructive interference;
3. $\psi_i = 60°$ and $d/D = 1.20$ transition between constructive and destructive;
4. $\psi_M = 45°$ and $d/D = 1.20$ corresponding to constructive interference.

In these three conditions, the nature of the signal changes completely, in particular, for one specific condition the signal becomes strongly time-dependent.

3.3.1 Noise intermittency: attractors and recurrence plot A major challenge in constructing a reliable recurrence plot (RP) and performing its quantification through recurrence quantification analysis (RQA) lies in the presence of the signal's stochastic component, which can obscure the underlying deterministic structure. This noise disrupts and deviates the diagonal lines, biasing the RQA measures based on these lines and potentially leading to misleading conclusions [34].
For this reason, the data decomposition technique which separates coherent and stochastic components, is particularly useful for the subsequent application of non linear analysis. For a more comprehensive understanding, numerous studies are available in the literature, including [19]. However, a short description of the data analysis strategy is provided in this paragraph.

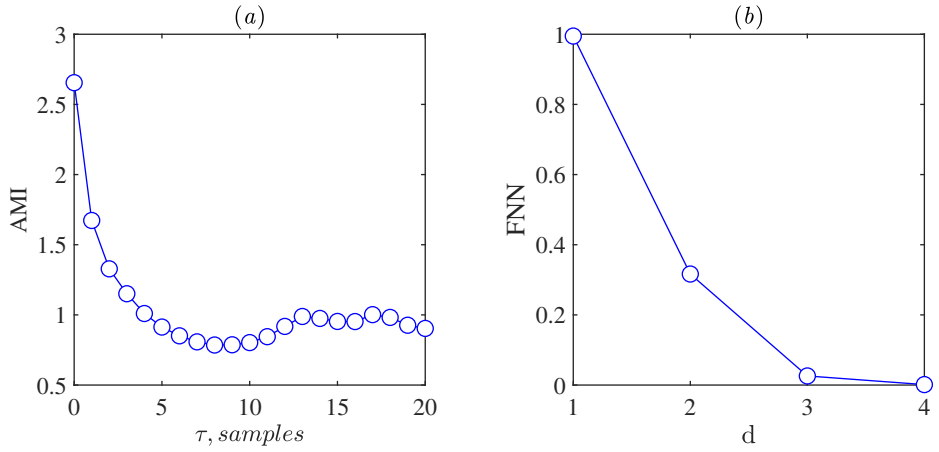

Figure 10: Average mutual information (a) and percentage of false nearest neighbours (b) used to determine the optimal time delay and embedding dimension, respectively. The time delay corresponds to the first minimum of the mutual information curve, while the optimal embedding dimension is identified where the percentage of false neighbours approaches zero.

The first minima of the Average Mutual Information (AMI) in Figure 10 (a) is the time delay recommended for phase space recostruction. The reconstruction matrix, constructed using the optimal time delay τ, can be expressed as follows::

$$y_i(d) = (x_i, x_{i+\tau}, ..., x_{i+(d-1)\tau}) \tag{1}$$

where, $i = 1, 2, ..., N_0 - (d-1)\tau$, N_0 is the length of the signal, x_i is the time-series, y_i is the i-th reconstructed vector, d is the embedding dimension, and τ is the time delay. To avoid spurious trajectory crossings in the reconstructed phase space due to an insufficient embedding dimension, it is crucial to determine the optimal embedding dimension. This is achieved by calculating false nearest neighbors FNN percentage across as the embedding dimension increases; the optimal dimension is identified when this percentage approaches zero. As shown in Figure 10(b), the system dynamics are effectively confined within a four-dimensional phase space.

The dominant features of the attractor can also be visualised as a three-dimensional projectio, which preserves most of the information regarding the system dynamics, or alternatively by using a two-dimensional Poincaré section, as depicted in Figures 11 (a, b, d, e, g, h, j, k).

In Figure 11 (a, b), the pressure trajectories in the pseudo-phase space come bacl to the same points after a period, making them recurrent. For this reason, in Figure 11 (c), the recurrence map shows well-defined and evenly spaced diagonals. The attractor does not describe a simple circular orbit; instead, it exhibits additional winding attributed to the presence of a harmonic component at twice the fundamental frequency, characterized by an high energy content. This phenomenon is related to the presence of the pylon inducing installation effects.

In Figures 11 (d, e), at $\psi_m = 15°$ (destructive interference), the attractor exhibits a spiral orbit around a closed loop: a toroidal attractor. This attractor topology indicates a complex structure due to multi-frequency dynamics. The shape of the attractor, compared to the isolated rotor, changes significantly in the case of destructive interference.

At $\psi_i = 60°$, the attractor returns to exhibits the similar structure observed for isolated rotor. The behaviour at $\psi_i = 60°$ where the attractor exhibits quasi-periodicity reflects a complex dynamical regime where the system's trajectories do not repeat but densely fill a certain region in the phase space. Trajectories of this type, which form a band in phase space, are typical of attractors describing chaotic phenomena such as Rössler and Lorentz. Thus, near constructive interference, the phenomenon becomes chaotic. The recurrence map shows clearer regions, evidencing a loss of recurrence (see Figure 11 (i)). This aspect is related to the intermittent nature of the second BPF.

As shown in Figures 11(j, k), at $\psi_M = 45°$, the attractor assumes the same geometry as the isolated rotor, indicating that under constructive interference, the rotors synchronize acoustically and behave like a single rotor. Compared to the isolated case, the trajectories are slightly further apart, and the recurrence map exhibits smaller clear zones. This latter aspect may be due to the control system intervening

to manage the phase shift between the propellers. As the interference transitions from destructive to constructive, the attractor expands and unfolds in the phase space, passing through a chaotic operating condition. This transition from destructive to constructive interference, both of which are linear dynamics, occurs by passing through a chaotic state, thus making it unpredictable through the solution of a mathematical model.

4 Conclusion

This investigation demonstrated the effectiveness of rotor phase synchronization as a passive noise reduction technique in co-rotating, side-by-side rotor configurations. Space-time Proper Orthogonal Decomposition (POD) successfully separated measured acoustic fields into tonal and broadband components, enabling precise analysis of acoustic interference mechanisms. Results revealed significant variations in noise levels due to constructive and destructive interference at specific phase angles, with notable reductions observed, particularly at second harmonic. Probability Density Function analyses confirmed clear distinctions in the statistical characteristics of pressure fluctuations, validating the decomposition technique's reliability. Overall, rotor synchronization emerged as a promising aeroacoustic control strategy, offering substantial noise mitigation potential.

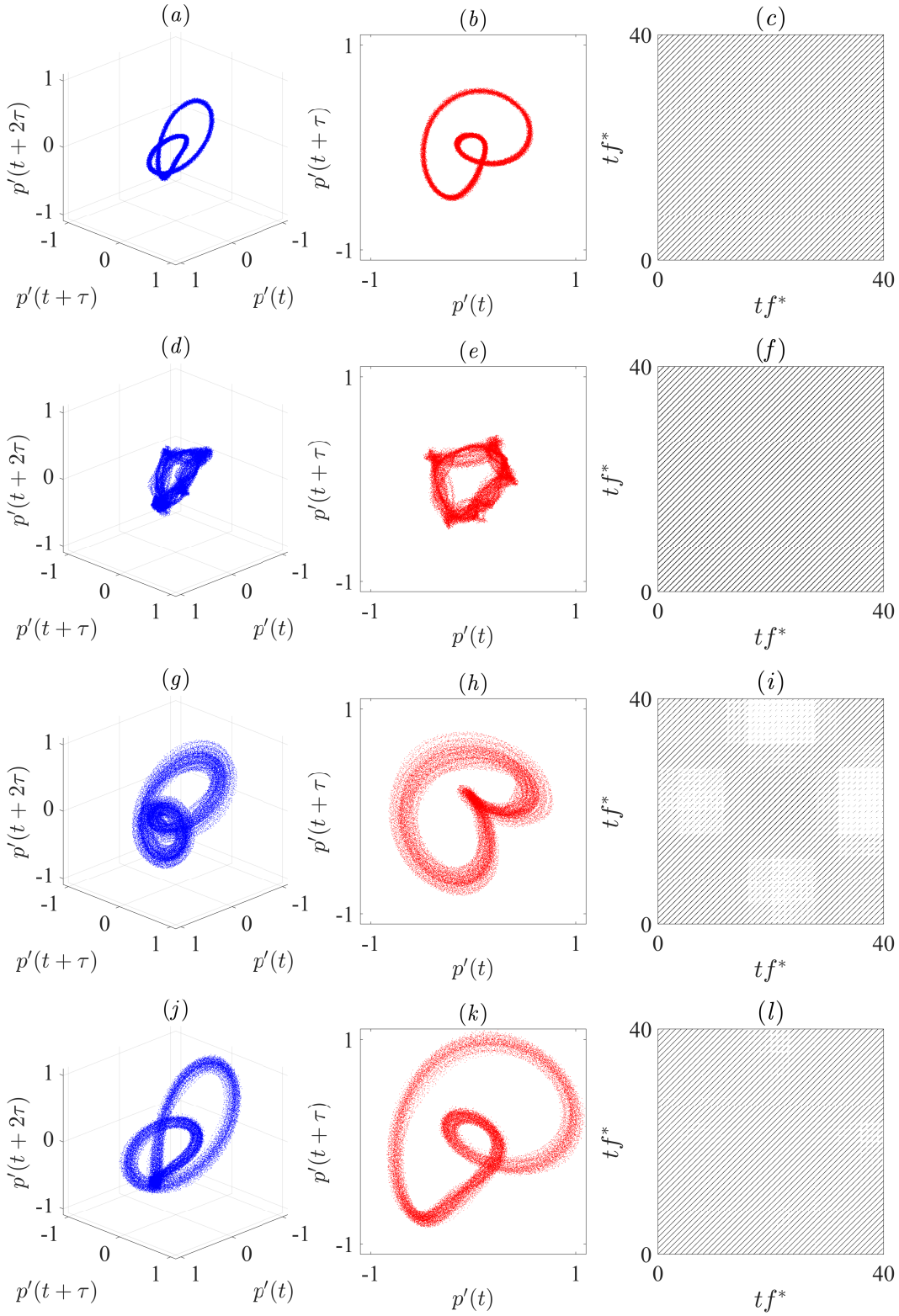

Figure 11: Three-dimensional (a, d, g, j) and two-dimensional (b, e, h, k) representations of the attractor in the pseudo-phase space; Recurrence plot. The first row shows the results for the single rotor, the second row illustrates the condition of destructive interference, the third row depicts the transition phase, and the last row presents the constructive interference.

5 Acknowledgments
Research activities described in the manuscript are part of the work carried out by the GARTEUR AG-26 consortium, which has promoted the collaboration between DLR and Niccolò Cusano University. We sincerely thank Prof. Patanè for implementing the rotor synchronization software.

References
[1] P. Bergé, M. Dubois, P. Mannevillel, and Y. Pomeau. Intermittency in Rayleigh-Bénard convection. *Journal de Physique Lettres*, 41(15):341–345, 1980.

[2] L. A. Bonomo, J. A. Cordioli, Alysson K. Colaciti, J. V. N. Fonseca, and L. G. C. Simões. A comparison of tonal-broadband decomposition algorithms for propeller noise. *Int. J. of Aeroacoustics*, 23(7-8):737–762, 2024.

[3] P. Candeloro, E. Martellini, R. Nederlof, T. Sinnige, and T. Pagliaroli. An experimental study of the aeroacoustic properties of a propeller in energy harvesting configuration. *Fluids*, 7(7):217, 2022.

[4] P. Candeloro, D. Ragni, and T. Pagliaroli. Small-scale rotor aeroacoustics for drone propulsion: A review of noise sources and control strategies. *Fluids*, 7(8):279, 2022.

[5] P. Candeloro, D. Ragni, and T. Pagliaroli. Unconventional application of serrated trailing edges for quieter propeller drones. In *30th AIAA/CEAS Aeroacoustics Conference (2024)*, page 3107, 2024.

[6] Paolo Candeloro, Edoardo Martellini, Robert Nederlof, Tomas Sinnige, and Tiziano Pagliaroli. An experimental study of the aeroacoustic properties of a propeller in energy harvesting configuration. *Fluids*, 7(7):217, 2022.

[7] Y. Cao, X. Huang, L. Sheng, and Z. Wang. A flight experimental platform for synchrophasing control based on a small propeller uav. *Sci. China Technological Sciences*, 61:1915–1924, 2018.

[8] A. Celik, N. S. Jamaluddin, K. Baskaran, S. Meloni, D. Rezgui, and M. Azarpeyvand. Experimental characterisation of rotor noise in tandem configuration. *Applied Acoustics*, 222:110053, 2024.

[9] L. Chengyi, W. Yafeng, and C. Geng. Active noise control experiment for unmanned aerial vehicle propeller. *Sci. Tech. and Eng.*, 14(9):1671–1815, 2014.

[10] T. Dbouk and D. Drikakis. Quadcopter drones swarm aeroacoustics. *Phys. Fluids*, 33(5), 2021.

[11] F. Del Duchetto, T. Pagliaroli, P. Candeloro, K.-S. Rossignol, and J. Yin. Aeroacoustic study of synchronized rotors. *Aerospace*, 12(2), 2025.

[12] S. Guan, Y. Lu, T. Su, and X. Xu. Noise attenuation of quadrotor using phase synchronization method. *Aerospace Sci. and Tech.*, 118:107018, 2021.

[13] Y. Guan, V. Gupta, and Larry K.B. Li. Intermittency route to self-excited chaotic thermoacoustic oscillations. *J. of Fluid Mech.*, 894:R3, 2020.

[14] O. Hertzman, S. Fligelman, and O. Stalnov. Abatement of a multi-rotor tonal noise component with phase control technology. In *28th AIAA/CEAS Aeroacoustics 2022 Conference*, page 2834, 2022.

[15] N. Intaratep, W. N. Alexander, W. J. Devenport, S. M. Grace, and A. Dropkin. Experimental study of quadcopter acoustics and performance at static thrust conditions. In *22nd AIAA/CEAS Aeroacoustics Conference*, page 2873, 2016.

[16] L. Kabiraj and R. Sujith. Nonlinear self-excited thermoacoustic oscillations: intermittency and flame blowout. *J. of Fluid Mech.*, 713:376–397, 2012.

[17] K. Kashinath, Larry K.B. Li, and M. P. Juniper. Forced synchronization of periodic and aperiodic thermoacoustic oscillations: lock-in, bifurcations and open-loop control. *J. of Fluid Mech.*, 838:690–714, 2018.

[18] K. Klimaszewska and J. J. Żebrowski. Detection of the type of intermittency using characteristic patterns in recurrence plots. *Phys. Rev. E*, 80:026214, Aug 2009.

[19] M. Marwan, M. C. Romano, M. Thiel, and J. Kurths. Recurrence plots for the analysis of complex systems. *Physics Reports*, 438:237–329, 2007.

[20] S. Meloni, E. de Paola, E. Grande, D. Ragni, L. G. Stoica, A. Di Marco, and R. Camussi. A wavelet-based separation method for tonal and broadband components of low reynolds-number propeller noise. *Measurement Science and Technology*, 34(4):044007, jan 2023.

[21] R. E. Nargi, P. Candeloro, F. De Gregorio, G. Ceglia, and T. Pagliaroli. Fluid-dynamic and aeroacoustic characterization of side-by-side rotor interaction. *Aerospace*, 10(10):851, 2023.

[22] T. Pagliaroli, P. Candeloro, R. Camussi, O. Giannini, G. Bella, and R. Panciroli. Aeroacoustic study of small scale rotors for mini drone propulsion: Serrated trailing edge effect. In *2018 AIAA/CEAS Aeroacoustics Conference*, page 3449, 2018.

[23] T. Pagliaroli, P. Candeloro, F. Del Duchetto, K.-S. Rossignol, and J. Yin. Exploring the effects of phase delay on propeller noise: an experimental study in tandem configuration. In *INTER-NOISE and NOISE-CON Congress and Conference Proceedings*, volume 270, pages 8565–8576. Institute of Noise Control Engineering, 2024.

[24] T. Pagliaroli and G. Troiani. Wavelet and recurrence analysis for lean blowout detection: An application to a trapped vortex combustor in thermoacoustic instability. *Physical Review Fluids*, 5(7):073201, 2020.

[25] Neel Pandey, John A Valdez, Wesley Beaman, and Charles E Tinney. Acoustics of side-by-side synchrophased rotors. In *30th AIAA/CEAS Aeroacoustics Conference (2024)*, page 3218, 2024.

[26] K.A. Pascioni, S.A. Rizzi, and N. Schiller. Noise reduction potential of phase control for distributed propulsion vehicles. In *AIAA Scitech 2019 Forum*, page 1069, 2019.

[27] A. Patterson, N. H. Schiller, K. A. Ackerman, A. Gahlawat, I. M. Gregory, and N. Hovakimyan. Controller design for propeller phase synchronization with aeroacoustic performance metrics. In *AIAA Scitech 2020 Forum*, page 1494, 2020.

[28] N. Platt, E.A. Spiegel, and C. Tresser. On-off intermittency: A mechanism for bursting. *Phy. Rev. Lett.*, 70(3):279, 1993.

[29] Y. Pomeau and P. Manneville. Intermittent transition to turbulence in dissipative dynamical systems. *Commun. Math. Phys.*, 74(2):189–197, 1980.

[30] M. Shao, Y. Lu, X. Xu, S. Guan, and J. Lu. Experimental study on noise reduction of multi-rotor by phase synchronization. *J. of Sound and Vib.*, 539:117199, 2022.

[31] C. E Tinney, Y. Zhao-Dubuc, and J. Valdez. The space-time structure of sound produced by stacked rotors in hover using vold-kalman filters and proper orthogonal decomposition. *International Journal of Aeroacoustics*, 22(5-6):576–598, 2023.

[32] B. Turhan, H. K. Jawahar, A. Gautam, S. Syed, G. Vakil, D. Rezgui, and M. Azarpeyvand. Acoustic characteristics of phase-synchronized adjacent propellers. *The Journal of the Acoustical Society of America*, 155(5):3242–3253, 2024.

[33] A. Visingardi, M. Barbarino, F. De Gregorio, L. Greco, C. Testa, S. Zaghi, J. Yin, G. Reboul, A. Cavalli, D. Granata, et al. Analysis of the aeroacoustic performance of twin propellers in hover by using the cira-cusano test-rig. In *European Rotorcraft Forum (ERF 2024)*, 2024.

[34] D. Wendi and N. Marwan. Extended recurrence plot and quantification for noisy continuous dynamical systems. *Chaos: An Interdisciplinary Journal of Nonlinear Science*, 28(8), 2018.

[35] S. Zhong, P. Zhou, W. Chen, H. Jiang, H. Wu, and X. Zhang. An investigation of rotor aeroacoustics with unsteady motions and uncertainty factors. *J. of Fluid Mech.*, 956:A16, 2023.